INAF/OATs
LFI Project System Team

Planck LFI

TITLE: **Planck/LFI: Beam Pattern Integrated over the Bandwidth**

DOC. TYPE: Technical Note
PROJECT REF.: PL-LFI-OAT-TN-088 PAGE: 1 of 30
ISSUE/REV.: 0.6 DATE: May 9, 2012

Prepared by	M.Maris, M.Sandri, F.Villa	May 9, 2012
Agreed by	M. Bersanelli LFI Instrument Scientist A. Zacchei LFI/DPC manager C.R. Butler LFI Program Manager	
Approved by	N. Mandolesi LFI Principal Investigator	

CHANGE RECORD

Issue	Date	Sheet	Description of change	Release
0.0	Mar 30, 2012	All	First draft of document	0.0
0.1	Apr 11, 2012	All	Introduced GRASP definition of directivity	0.1
0.2	Apr 13, 2012	All	Number assigned	0.2
0.3	Apr 24, 2012	All	Added results of gaussian fit	0.3
0.4	Apr 26, 2012	All	Added results of montecarlos	0.4
0.5	Apr 27, 2012	All	Improved text, first release on the twiki	0.5
0.6	May 9, 2012	All	Some typos corrected. Introduced some example map of averaged beams.	0.6

DISTRIBUTION LIST

Recipient	Company/Institute	E-mail address	Sent
Michele Maris	INAF/OATS	maris@oats.inaf.it	May 9, 2012
Samuele Galeotta	INAF/OATS	galeotta@oats.inaf.it	May 9, 2012
Andrea Zacchei	INAF/OATS	zacchei@oats.inaf.it	May 9, 2012
Marco Frailis	INAF/OATS	frailis@oats.inaf.it	May 9, 2012
Maura Sandri	INAF/IASFBO	sandri@iasfbo.inaf.it	May 9, 2012
Fabrizio Villa	IVilla/IASFBO	villa@iasfbo.inaf.it	May 9, 2012

Contents

LIST OF ABBREVIATIONS

acronym	**Explanation**
DMC	Data Management Component
FPdb	Focal Plane database
HFI	High Frequency Instrument
IT	Information Technology
LFI	Low Frequency Instrument
LOS	Line–of–Sight
RF	Referece Frame
PoV	Point of View
SotA	State of the Art
SSB	Solar System Baricenter
SSO	Solar System Object
TBC	To Be Confirmed
TBD	To Be Defined
TOD	Time Ordered Data
TODs	Plural of TOD
TOI	Time Ordered Information
TODs	Plural of TOI

1 Applicable and Reference Documents

Applicable Documents

[AD-1] New Astro., 7, 483 (2010), *Asteroid detection with millimetric wavelengths with the PLANCK survey* Cremonse, G., Marzari, F., Burigana, C., Maris, M.

Reference Documents

[AD-2] Journal of Instrumentation, Volume 12, Issue 12, pp. T12010 (2009), *Planck-LFI radiometers' spectral response* Zonca, A.; Franceschet, C.; Battaglia, P.; Villa, F.; Mennella, A.; D'Arcangelo, O.; Silvestri, R.; Bersanelli, M.; Artal, E.; Butler, R. C.; Cuttaia, F.; Davis, R. J.; Galeotta, S.; Hughes, N.; Jukkala, P.; Kilpi, V.-H.; Laaninen, M.; Mandolesi, N.; Maris, M.; Mendes, L.; Sandri, M.; Terenzi, L.; Tuovinen, J.; Varis, J.; Wilkinson, A.

[RD-1] A&A, 520, A2, 2010 *Planck pre–launch status: The optical system* Tauber,J.A, et al

[RD-2] Unknown Author,2009 *Planck/LFI DPC: LFI RIMO* Planck/LFI Int.Rep.: PL-LFI-OAT-TN-unknown, Issue 8.1, December 2009

[RD-3] Knud Pontoppidan *GRASP Technical Description* 2005, TICRA

[RD-4] Pablo Fosalba[1], Arturo Martín Polegre[2] *Conventions and Coordinate Systems for the Polarized Radiation Patterns Simulated at ESTEC using GRASP8* Unnumbered document ESTEC, November 22, 2000

[RD-5] Unknown Author ,2000 *Planck Telescope Design Specification* Internal Report ESTEC/SCI-PT-RS-07024, 31 August 2000

[RD-6] M. Sandri, F. Villa *Planck/LFI: Main Beam Locations and Polarization Alignment for the LFI Baseline FPU* PL-LFI-PST-TN-027 July, 2001

[RD-7] M. Sandri *Bandwidth dependence of LFI main beams* PL-LFI-PST-TN-075 October 23, 2006

[RD-8] M. Sandri, F. Villa *LFI Main Beams at 30 GHz* PL-LFI-PST-TN-040 February 22, 2005

[RD-9] M. Sandri *LFI Beams Delivery Format Specifications* PL-LFI-PST-TN-044 July 15, 2003

[RD-10] M. Sandri, F. Villa *LFI Main Beams at 44 GHz* PL-LFI-PST-TN-061 February 22, 2005

[RD-11] M. Sandri, F. Villa *LFI Main Beams at 70 GHz* PL-LFI-PST-TN-062 February 22, 2005

2 Scope of the document

We want to estimate the effect of a frequency dependent beam patter $\mathcal{D}_\nu(\hat{\gamma})$ on the detection of a source of spectrum $\mathcal{S}(\nu)$ taking in account the radiometer efficiency at frequency ν $\tau(\nu)$.

2.1 Limits of Applicability

In the following ν is a frequency, while f is an index to define a frequency channell.

Unless stated the reference system considered here is the Beam Reference Frame, whose Z axis is the main beam axis.

Limitations for Issue 0.4

1. the reflection loss (see App. A) is just estimated not considered.
2. Beam smearing is not taken in account.
3. The number of beam maps at different frequencies within the bandpass is rather limited, both as a number of maps and as a frequecy coverage.
4. The intent of the current issue it to estimate the level of effect of bandpass integration then to provide SotA corrections to be applied to real data.

3 Introduction

A point source at frequency ν seen in $\hat{\gamma}$ is represented here by a Dirac's Delta $\mathcal{S}(\nu)\delta(\hat{\gamma}' - \hat{\gamma})$. Extendend sources can be modelled as sums of point sources. In general we will consider a SED represented by a power–law so that

$$\mathcal{S}(\nu) = \mathcal{S}_{\rm ref}\nu^{\alpha}; \tag{1}$$

with α the spectral index, $\nu_{\rm ref}$ a reference frequency, $\mathcal{S}_{\rm ref}$ the spectral density at the reference frequency.

The beam-pattern $\mathcal{D}_\nu(\hat{\gamma})$ gives the amount of energy transferred from space to the radiometer when observing a source at frequency ν. In our case the amount of radiation transferred from the space to the radiometer would be formally

$$\mathcal{S}_{\rm opt}(\nu,\hat{\gamma}) = \mathcal{S}(\nu)\int_{4\pi} d^3\hat{\gamma}'\ \mathcal{D}_\nu(\hat{\gamma}')\delta(\hat{\gamma}' - \hat{\gamma}); \tag{2}$$

which leads to the obvious

$$\mathcal{S}_{\rm opt}(\nu,\hat{\gamma}) = \mathcal{D}_\nu(\hat{\gamma})\mathcal{S}(\nu); \tag{3}$$

The radiometer converts a power into a voltage with a linear transform whose slope is called Gain, G which can be expressed as an example in units of Volts over Watts. The Gain can be factorised into two parts G of which just one is a function of frequency, in general those parts are consider as a whole but here we will left them separed. So we have at a given frequency $G(\nu) = G_{\rm W2V}\tau(\nu)$ with

1. $G_{\rm W2V}$ the power to voltage conversion factor ;
2. and $\tau(\nu)$ the radiometer efficiency at frequency ν.

The $\tau(\nu)$ measures the ability of the radiometer to convert the energy of a radiowave at frequency ν into an electric signal, so the amount of power per unit frequency intervall observed by a radiometer at frequency ν is

$$\mathcal{S}_{\rm rad}(\nu,\hat{\gamma}) = \tau(\nu)\mathcal{D}_\nu(\hat{\gamma})\mathcal{S}(\nu); \tag{4}$$

after that the conversion to a sensed voltage is obtained by integrating over the frequency band $[\nu_1,\nu_2]$ and scaling by the appropriate $G_{\rm W2V}$ factor

$$V(\hat{\gamma}) = G_{\rm W2V}\int_{\nu_1}^{\nu_2} d\nu\ \tau(\nu)\mathcal{D}_\nu(\hat{\gamma})\mathcal{S}(\nu); \tag{5}$$

In our case we take the $\tau(\nu)$ from the RIMO is normalized by a factor N_τ

$$N_\tau^{-1} = \int_{\nu_1}^{\nu_2} d\nu\ \tau(\nu); \tag{6}$$

to have unit integral, this coefficient being usually included into $G_{\rm W2V}$. Also the $\mathcal{D}_\nu(\hat{\gamma})$ can be normalized in different ways in our case we follow the GRASP convention which defines $D_\nu(\hat{\gamma})$ as a *directivity* [1]

$$D_\nu(\hat{\gamma}) := 4\pi\frac{P_d(\hat{\gamma})}{P_{\rm in}} \tag{7}$$

where $P_{\rm in}$ is the power injected in the telescope by the feedhorn, $P_d(\hat{\gamma})$ is the power irradiated by the antenna toward $\hat{\gamma}$ over the unit solid angle, so that [2].

$$\int_{4\pi} d^3\hat{\gamma} D_\nu(\hat{\gamma}) = 4\pi. \tag{8}$$

The normalization constant can be included in the $G_{\rm W2V}$ coefficient too giving [3]

$$V(\hat{\gamma}) = G_{\rm W2V}\int_{\nu_1}^{\nu_2} d\nu\ \bar{\tau}(\nu)D_\nu(\hat{\gamma})\mathcal{S}(\nu). \tag{9}$$

In the following we are not - yet - intersted in considering the conversion to a voltage, so we will assume $G_{\rm W2V} = 1$ and we will determine the spectral averaged power [4]

$$\bar{\mathcal{S}}(\hat{\gamma}) = \frac{1}{\Delta\nu_{\rm eff}(\hat{\gamma})}\int_{\nu_1}^{\nu_2} d\nu\ \bar{\tau}(\nu)D_\nu(\hat{\gamma})\mathcal{S}(\nu); \tag{10}$$

with

$$\Delta\nu_{\rm eff}(\hat{\gamma}) = \int_{\nu_1}^{\nu_2} d\nu\ \bar{\tau}(\nu)D_\nu(\hat{\gamma}). \tag{11}$$

[1] See [RD-3] page 273, Eq. (4.1-20) and following.

[2] Other valid conventions are to impose either $\int_{4\pi} d^3\hat{\gamma}\ D_{\nu_0}(\hat{\gamma}) = 1$ or to normalize at the peak value at some reference frequency to have $D_{\nu_0}(\hat{\mathbf{0}}) = 1$ (or some other reference value) giving $D_\nu(\hat{\gamma}) = \mathcal{D}_\nu(\hat{\gamma})/\mathcal{D}_{\nu_0}(\hat{\mathbf{0}})$. The $\mathcal{D}_{\nu_0}(\hat{\mathbf{0}})$ can be included in the $G_{\rm W2V}$ coefficient.

[3] It has to be noted that in GRASP maps the loss of powert due to reflection is not included. Appendix A gives an estimate valid just for the current issue (0.4) of the document which shows the effect to be quite small.

[4] Note that in case we impose $\bar{\tau}(\nu) \equiv 1$ and $D_\nu(\hat{\gamma})$ to be independent of frequency then $\Delta\nu_{\rm eff} = \Delta\nu = \nu_2 - \nu_1$ and Eq. (10) reduces to $\bar{\mathcal{S}}(\hat{\gamma}) = (D(\hat{\gamma})/\Delta\nu)\int_{\nu_1}^{\nu_2} d\nu\ \mathcal{S}(\nu)$.

A convenient way to describe the spectral response of the instrument is to give its central frequency f_c and bandwidth $\Delta\nu$. Of course for a top–hat frequency window

$$\begin{array}{rcl} f_c & = & \frac{\nu_2+\nu_1}{2}; \\ \Delta\nu & = & \nu_2-\nu_1; \end{array} \tag{12}$$

while for a not uniform spectral distribution a spectral weight has to be introduced $w(\nu)$ leading to

$$\begin{array}{c} f_c = \frac{\int_{\nu_1}^{\nu_2} \nu w(\nu) d\nu}{\int_{\nu_1}^{\nu_2} w(\nu) d\nu}; \\ \Delta\nu = \left[12 \frac{\int_{\nu_1}^{\nu_2} \nu^2 w(\nu) d\nu}{\int_{\nu_1}^{\nu_2} w(\nu) d\nu} - f_c^2\right]^{0.5}. \end{array} \tag{13}$$

which in the limit of $w(\nu) \equiv 1$ backs to Eq. (12). Depending on the effect to consider we may play with different combinations of $\bar{\tau}(\nu)$, $D_\nu(\hat{\gamma})$ and $\mathcal{S}(\nu)$ in defining $w(\nu)$. Note that in principle if $D_\nu(\hat{\gamma})$ is included f_c and $\Delta\nu$ are a function of $\hat{\gamma}$, so either an average on the beam has to be consider or the peak value on the main beam.

Let be to denote with I_0 the brightness of a source scaling as ν^α and with I'_0 the brightness derived from the measures in the hypothesis that the beam pattern is frequency independent, ideally $I'_0/I_0 = 1$, but having not accouted for the spectral dependence of the beam pattern a bias will be introduced. The brightness can be derived from the power integrated over tha bandwidth

$$W(\hat{\gamma}) = I_0 \int_{\nu_1}^{\nu_2} d\nu\, \tau(\nu) D_\nu(\hat{\gamma}) \nu^\alpha; \tag{14}$$

or its spectral average

$$\bar{\mathcal{S}}(\hat{\gamma}) = \frac{I_0}{\Delta\nu} \int_{\nu_1}^{\nu_2} d\nu\, \tau(\nu) D_\nu(\hat{\gamma}) \nu^\alpha; \tag{15}$$

Despite equivalent the two definitions leads to two different bias, we will denote with b_W the bias derived from W and with b_S the biad derived from $\bar{\mathcal{S}}$.

Let be to define with $D_{\mathbf{ref}}(\hat{\gamma})$ a monochromatic beam pattern assumed to be representative of the real beam pattern in sky, and let be to denote with W_O the observed integrated power and with W_M the model integrated power then

$$W_O(\hat{\gamma}) = I_0 \int_{\nu_1}^{\nu_2} d\nu\, \tau(\nu) D_\nu(\hat{\gamma}) \nu^\alpha;$$

$$W_M(\hat{\gamma}) = I'_0 D_{\mathbf{ref}}(\hat{\gamma}) \int_{\nu_1}^{\nu_2} d\nu\, \tau(\nu) \nu^\alpha;$$

then by equating the two powers and defining bias as I'_0/I_0

$$b_W(\hat{\gamma}) = \frac{\int_{\nu_1}^{\nu_2} d\nu\, \tau(\nu) D_\nu(\hat{\gamma}) \nu^\alpha}{D_{\mathbf{ref}}(\hat{\gamma}) \int_{\nu_1}^{\nu_2} d\nu\, \tau(\nu) \nu^\alpha}; \tag{16}$$

in a similar manner after defining as $\Delta\nu_{\mathrm{eff,O}}(\hat{\gamma})$ the effective bandwidth for the observed data, and $\Delta\nu_{\mathrm{eff,M}}$ as the effective bandwidth for the model, the bias for the spectral averaged intensity is

$$b_S(\hat{\gamma}) = \frac{\Delta\nu_{\mathrm{eff,M}}}{\Delta\nu_{\mathrm{eff,O}}(\hat{\gamma})} \frac{\int_{\nu_1}^{\nu_2} d\nu\, \tau(\nu) D_\nu(\hat{\gamma}) \nu^\alpha}{D_{\mathbf{ref}}(\hat{\gamma}) \int_{\nu_1}^{\nu_2} d\nu\, \tau(\nu) \nu^\alpha}; \tag{17}$$

At last from the power it is possible to extract the antenna temperature given $I_0 \propto T_{\mathbf{ant}} G_{T\mathrm{ant}2W}$ with the $G_{T\mathrm{ant}2W}$ defined as

$$G_{T\mathrm{ant}2W} = f_{\mathrm{c}}^2 \Delta\nu / \mathrm{FWHM}^2. \tag{18}$$

A systematic error in estimating $G_{T\mathrm{ant}2W}$ arising from any of the parameters $\Delta\nu$, f_{c} or FWHM will lead to a relative bias in the antenna temperature $b_{T\mathrm{ant}} = T'_{\mathbf{ant}}/T_{\mathbf{ant}} - 1 = 1 - G'_{T\mathrm{ant}2W}/G_{T\mathrm{ant}2W}$. If the three quantities $\Delta\nu$, f_{c} or FWHM would change indepedently the bias would be

$$b_{T\mathrm{ant}} \approx -2\frac{\delta f_{\mathrm{c}}}{f_{\mathrm{c}}} - \frac{\delta\Delta\nu}{\Delta\nu} + 2\frac{\delta\mathrm{FWHM}}{\mathrm{FWHM}}. \tag{19}$$

but in this case those three quantities are correlated being connected to the same cause.

4 A test example

We considered here a test example for 27 X with the GRASP beam for the frequency 28.5 GHz is at top of Fig. 1, while the averaged beam derived averaging over $\bar{\tau}(\nu)\mathcal{S}(\nu)$ with $\alpha = 0$ is shown at bottom. Plots of $D_\nu(\hat{\mathbf{0}})$ and $\bar{\tau}(\nu)$ are in Fig. 2.

It is evident how there is a relative change in the peak power of about 6% as a function of frequency equivalent to a peak–to–peak change of about 0.3 dbi. This change is connected both to the effect of diffraction and changes in the illuminated fraction of secondary mirror.

The Fig. **??** compares the variability of GRASP beams as a function of frequency with respect to the variability of averaged beams as a function of α it is evident as some of the oddities in the GRASP beams have been reduced by averaging over the bandpass. Also the level of across the range of α values is smaller than across the range of frequencies.

4.1 Frequency Center

We are here interested at first in finding the changes in f_c and $\Delta\nu$, as we introduced the various components of the radiometer and telescope responsivity. Fig. 4 shows how the central frequency changes as a function of α. Integrals are all defined within the frequency range of Fig. 2. Comparing the different versions of averages it is evident how the beam changes just slightly the central frequency, most of the effect indeed is produced by the integration over the bandwidth and by the effect of the spectral index. Fig. 5 gives the variation of f_c when different components are used in the integral. The green line refers to the change of f_c by taking $\mathcal{S}(\nu)\bar{\tau}(\nu)D_\nu(\hat{\mathbf{0}})$ with respect to the case in which just $\bar{\tau}(\nu)$ is taken in account. Changes of up to a 2% with respect to the case of just bandpass are required changing α. However the red line compares the same variation with respect to the case in which the beam is not included (i.e. $\mathcal{S}(\nu)\bar{\tau}(\nu)$ v.z. $\bar{\tau}(\nu)$), while the blue line compares $\bar{\tau}(\nu)D_\nu(\hat{\mathbf{0}})$ v.z. $\bar{\tau}(\nu)$). The effect of beam seems quite small in this case.

4.2 Band Width

Fig. 6 shows the effect of averaging over the bandpass as a function of spectral index and of the components introduced in the integral. Blue line with dots is the integral perfomed over top hat. Magenta line with leftward triangles including $D_\nu(\hat{\mathbf{0}})$. Green line with downward triangles includes just $N\tau(\nu)$. The yellow line with rightward triangles includes $D_\nu(\hat{\mathbf{0}})\bar{\tau}(\nu)$. The red line with squares is the effect of the spectrum alone. The black line with squares includes also $\mathcal{S}(\nu)D_\nu(\hat{\mathbf{0}})$. Light blue and dark blue lines are for $\mathcal{S}(\nu)\bar{\tau}(\nu)$. and $\mathcal{S}(\nu)\bar{\tau}(\nu)D_\nu(\hat{\mathbf{0}})$.

In all the cases the difference between the effective bandwidth when including the frequency dependence of $D_\nu(\hat{\mathbf{0}})$ is about 1.5%, with a slight dependence on α. This is well shown in Fig. 7 where the relative change in the $\Delta\nu_{\rm eff}$ when including or not $D_\nu(\hat{\mathbf{0}})$ is plotted.

4.3 Integrated Power

Given the beam response changes with γ all the quantities discussed in the sections above changes with the position of the source with respect to the beam. This shown here while discussing $b_{\rm W}$ in Fig. 8 and its enlargement in Fig. 9 giving the $b_{\rm W}$ as a function of α. The bias is a function of the position of the source on the beam, but its distribution is flat on the main beam and in any case the bias is within 1%. The figure takes the beam pattern at 30 GHz as a reference beam pattern. The amount of variability displayed by plots as those reported here are even a factor of two larger, than those shown here.

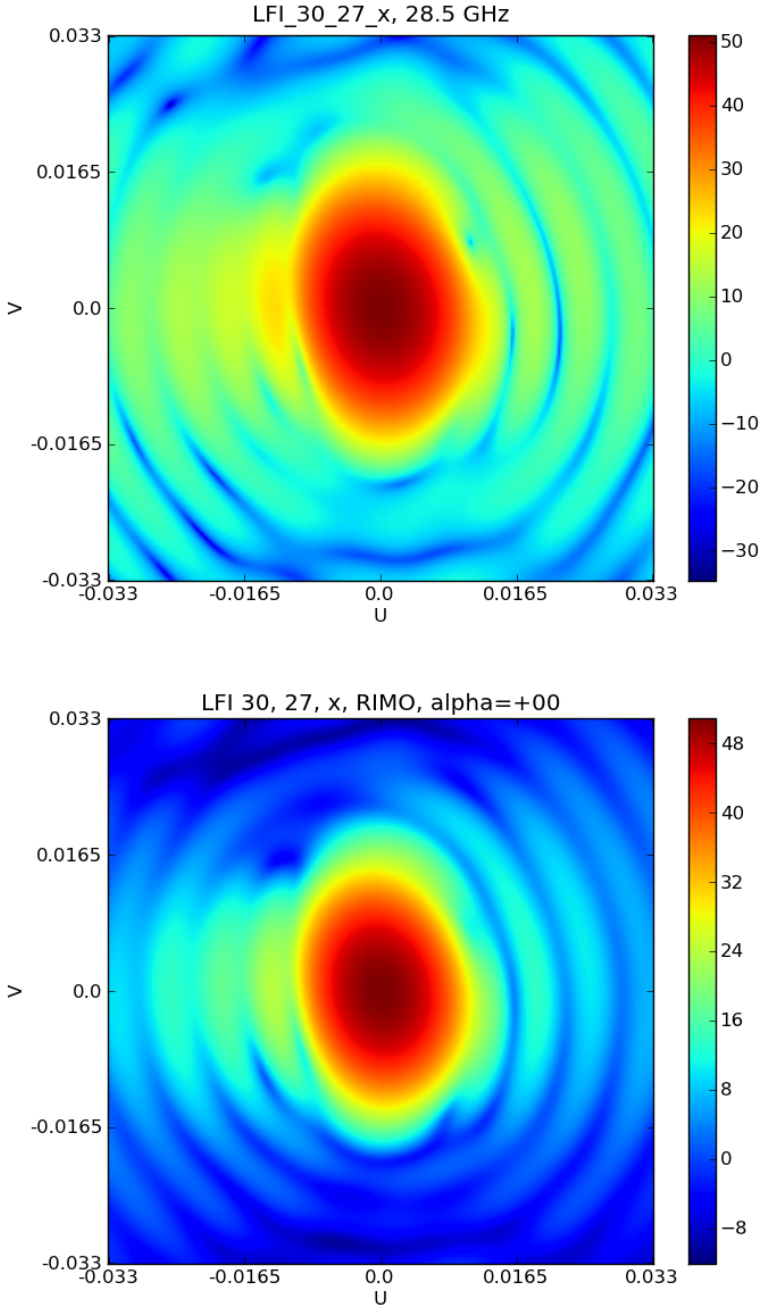

Figure 1: Top a GRASP beam for the LFI FH 27X at 28.5 GHz. Bottom the bandpass averaged beam for $\alpha = 0$ and the same frequecy channell.

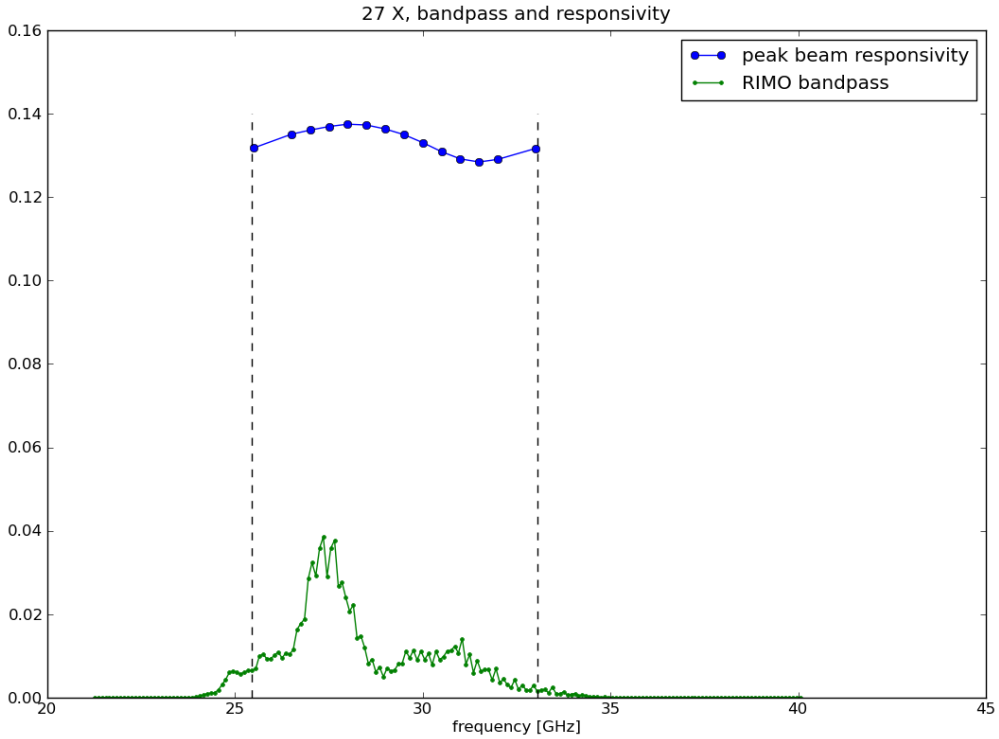

Figure 2: The normalized bandpass for 27 X from RIMO (green points) and the peak beam rensponsivity (blue points) $D_\nu(\hat{\mathbf{0}})$, arbitrarily scaled to fit the plot. The black lines mark the frequency intervall taken in consideration.

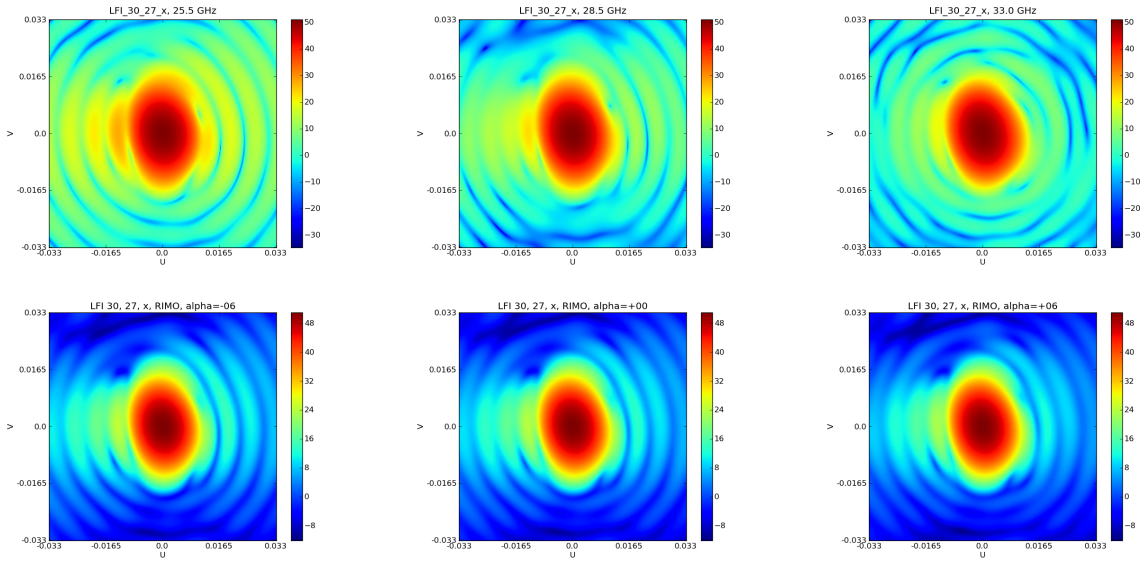

Figure 3: Top: variability of GRASP beams as a function of frequency. Bottom: variability of averaged beams as a function of α.

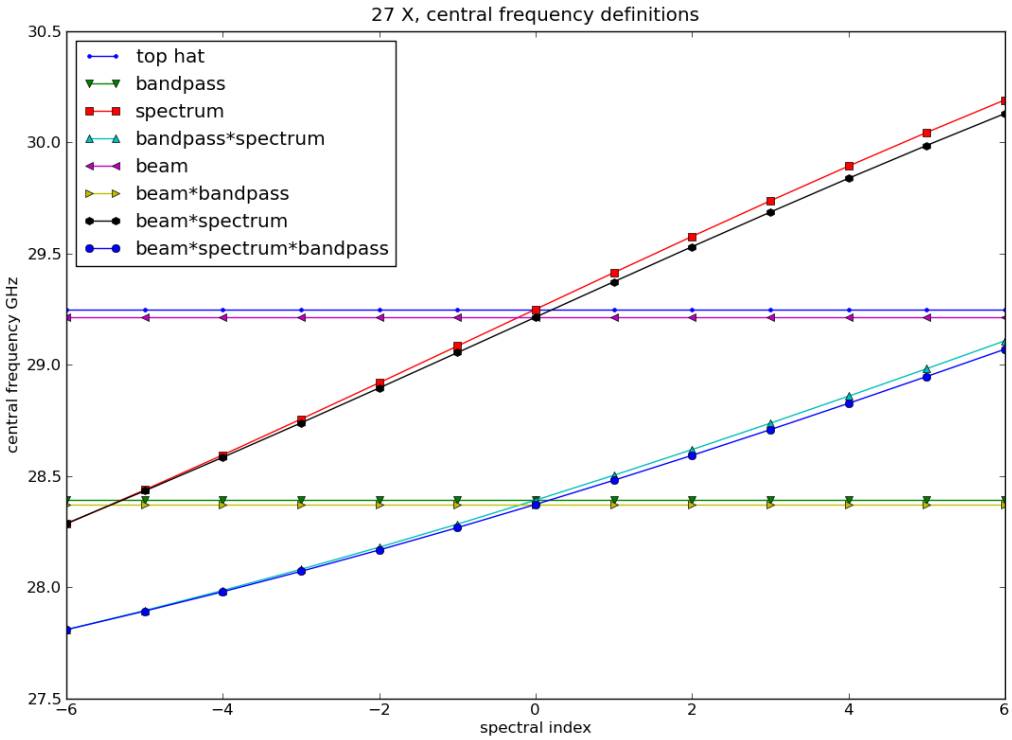

Figure 4: Central frequency as a function of spectral index α including the spectrum (red squares), the bandpass and the spectrum (light blue triangles), the beam peak responsivity and the spectrum (black circles) and the beam at peak responsivity, the spectrum and the bandpass (blue circles). As a reference the aforementioned combinations are displayed without to introduce the beam, so we have a top–hat (blue dots), the bandpass (green triangles), of the beam at peak value (red triangles), of the beam at peak value and band pass (yellow triangles).

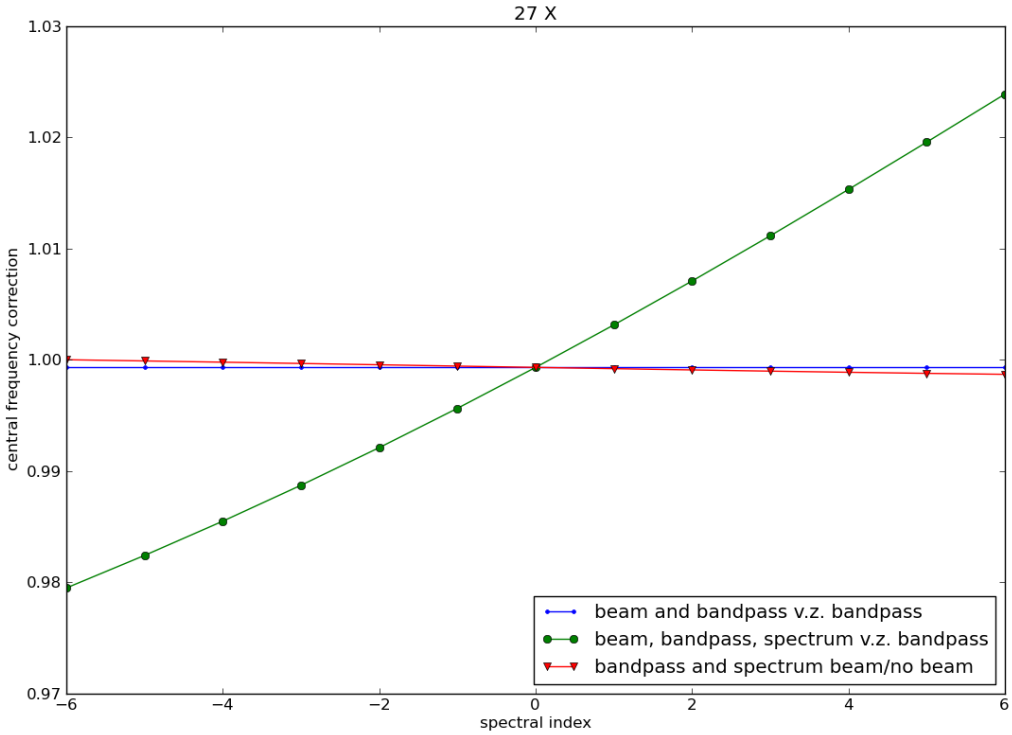

Figure 5: Green line (circles) f_c computed taking in account of the bandpass, spectrum and beam with respect to the case in which just the bandpass is considered. Red line (triangles) comparison of f_c computed taking in account of the bandpass, spectrum and beam with the case in which the beam is not considered. Blue line (dots) f_c computed taking in account of the bandpass, and beam compared to f_c computed just taking in account of the bandpass.

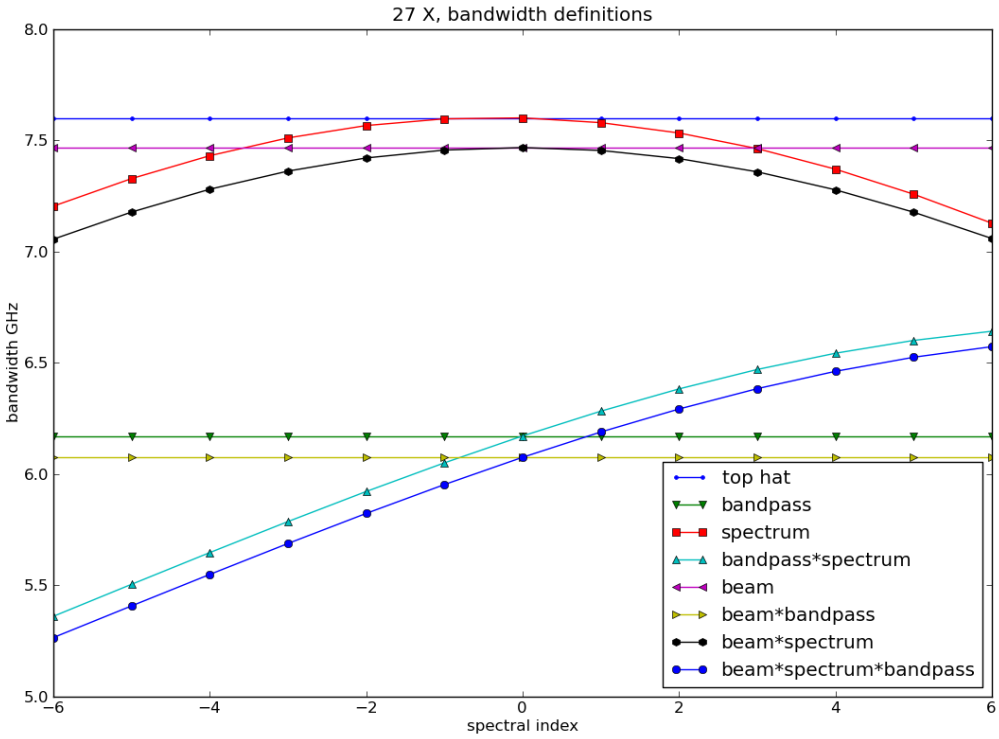

Figure 6: $\Delta\nu_{\rm eff}$ as a function of α and of the averaging. Blue line with dots the integral perfomed over top hat. Magenta line with leftward triangles integral over $D_\nu(\hat{\mathbf{0}})$. Green line with downward triangles integral over $\bar{\tau}(\nu)$. The yellow line with rightward triangles integral over $D_\nu(\hat{\mathbf{0}})\bar{\tau}(\nu)$. The red line with squares integral over $\mathcal{S}(\nu)$. The black line with squares integral over $\mathcal{S}(\nu)D_\nu(\hat{\mathbf{0}})$. Light blue line with upward triangles integral over $\mathcal{S}(\nu)\bar{\tau}(\nu)$. Dark blue line with squares integral over $\mathcal{S}(\nu)\bar{\tau}(\nu)D_\nu(\hat{\mathbf{0}})$.

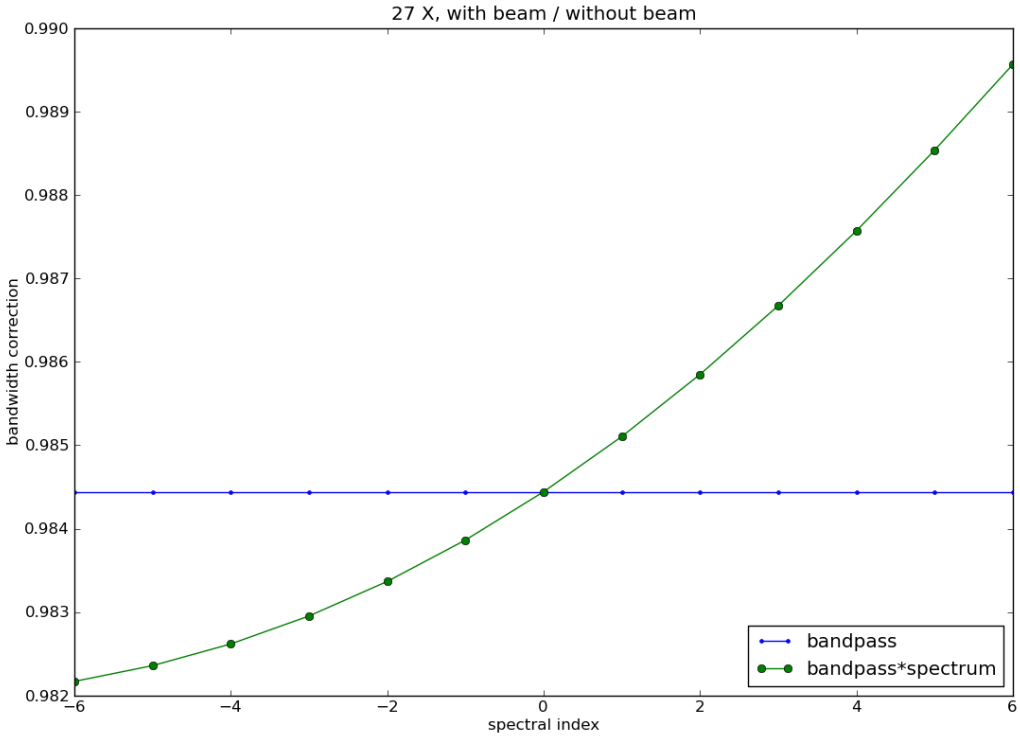

Figure 7: Relative change in the $\Delta\nu_{\rm eff}$ when including $D_\nu(\hat{\mathbf{0}})$ with respect to the case in which $\Delta\nu_{\rm eff}$ it is not included. Blue line with dots integral over $\bar{\tau}(\nu)$. Green line with circles integral over $\mathcal{S}(\nu)\bar{\tau}(\nu)$.

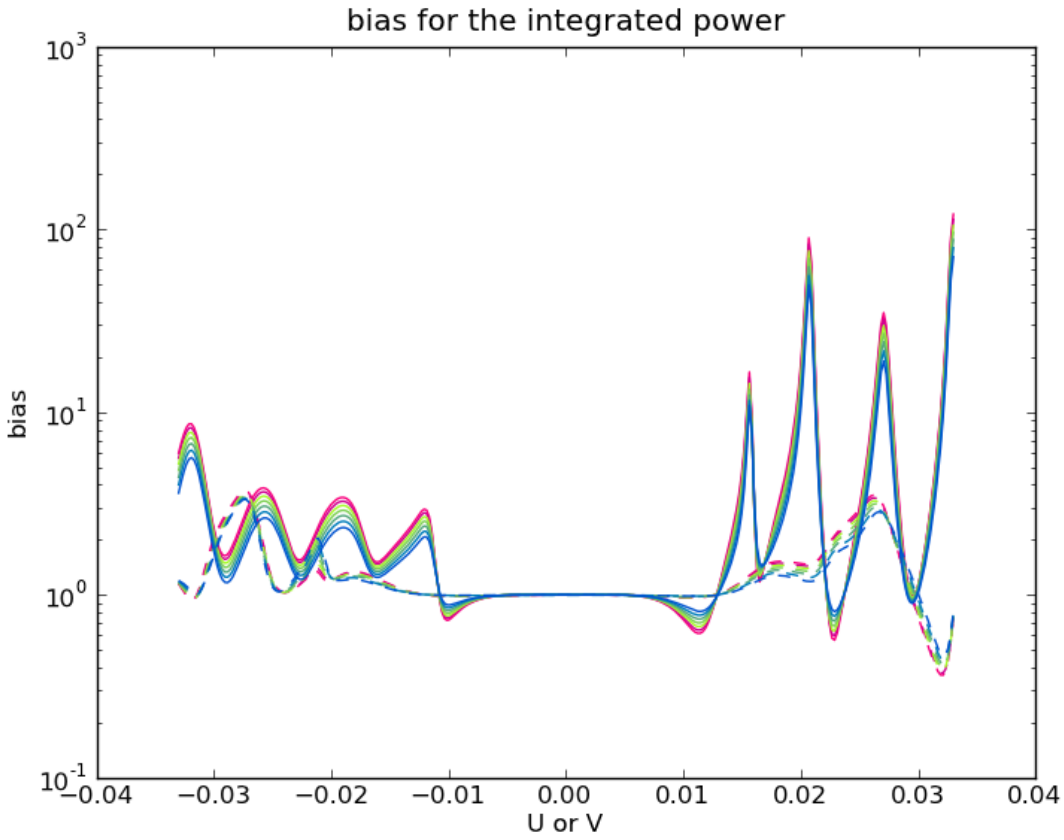

Figure 8: The b_W as a function of α for a cut along the U axis (full lines) or the V axis (dashed lines). Colours are scaled from red to blue for $\alpha = -6$, -4, -2, 0, +2, +4, +6.

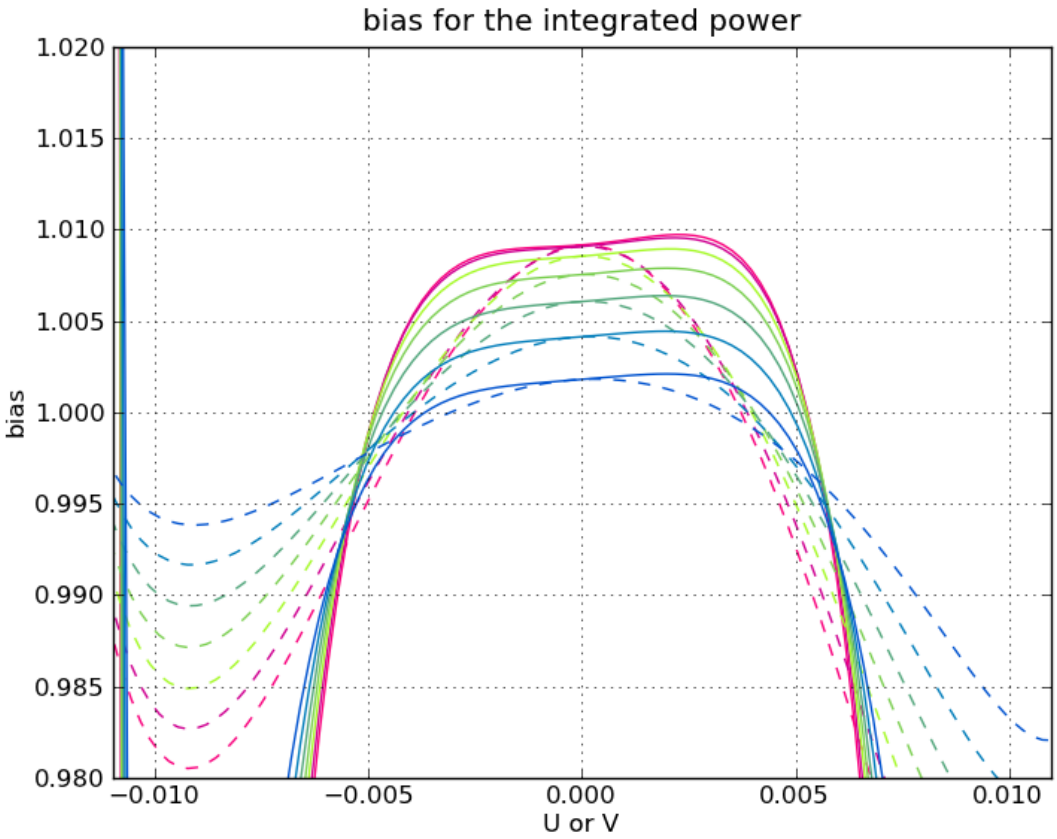

Figure 9: The b_W as a function of α for a cut along the U axis (full lines) or the V axis (dashed lines). Colours are scaled from red to blue for $\alpha = -6$, -4, -2, 0, +2, +4, +6. The figure is zoomed in the region of the main beam.

5 Montecarlo propagation of Bandpass Uncertaitinties

In the previous section Beam maps are integrated averaging by the RIMO bandpass, assuming different spectral indexes, α, ranging from -6 to 6 and without to account for beam smearing. In this section we address the question of how uncertaities over the bandpass propagates at the level of beams. This allows to asses the level of predictability of each of those parameters taking in account the uncertaities into the bandpass. The procedure is as follow:

1. A randomly generated bandpass is produced
2. Beam is integrated over that bandpass for a given source spectrum
3. Gaussian fit is estimated for that beam
4. Statistics are derived for a set of $n_{\rm mc}$ realizations for the results of the Gaussian fit

Critical details are reported in subsections 5.1 and subsection 5.2, while the results are in subsection 5.3.

5.1 Generation of a random bandpass

There is a lack of knowledge about the exact amount and statistics of uncertainties in the bandpass currently released in the RIMO 8.2. An estimate is reported in [AD-2] which quoted an uncertainty of 1.5 $-$ 2db as a fiducial value.

Given this level of uncertainty we studied a "worst–case" in which

1. each sample of the spectral response has an flat distribution of values;
2. each sample of the spectral response varies randomly in a way independent from each other:
3. the peak-to-peak relative variation is $\delta_{\rm db}\log\tau$;
4. $\delta_{\rm db}\log\tau$ has two possible values:

   $\delta_{\rm db}\log\tau = 2$ db corresponding to the hypothesis in which the quoted uncertainty in [AD-2] is the whole uncertainty;

   $\delta_{\rm db}\log\tau = 2\sqrt{12}$ db, which correspond to the case in which the quoted uncertainty in [AD-2] is 1σ.
5. It is assumed $\delta_{\rm db}\log\tau$ is constant across the bandpass.

5.2 Gaussian fit

Gaussian fit is perfomed by minimizing χ^2 for the averaged maps in the U, V plane against the model

$$G_{\rm m}(U,V) = g_0 \exp\left[-\frac{8\log 2}{2}\begin{pmatrix} U-U_0 \\ V-V_0 \end{pmatrix}^{\dagger} \mathbf{U}(-\psi_{\rm ell})\,{\rm diag}\left({\rm fwhm}_{\rm max}^{-2}, {\rm fwhm}_{\rm min}^{-2}\right)\mathbf{U}(\psi_{\rm ell})\begin{pmatrix} U-U_0 \\ V-V_0 \end{pmatrix}\right]. \tag{20}$$

with

$$\mathbf{U}(\psi_{\rm ell}) = \begin{pmatrix} \cos\psi_{\rm ell} & -\sin\psi_{\rm ell} \\ \sin\psi_{\rm ell} & \cos\psi_{\rm ell} \end{pmatrix}.$$

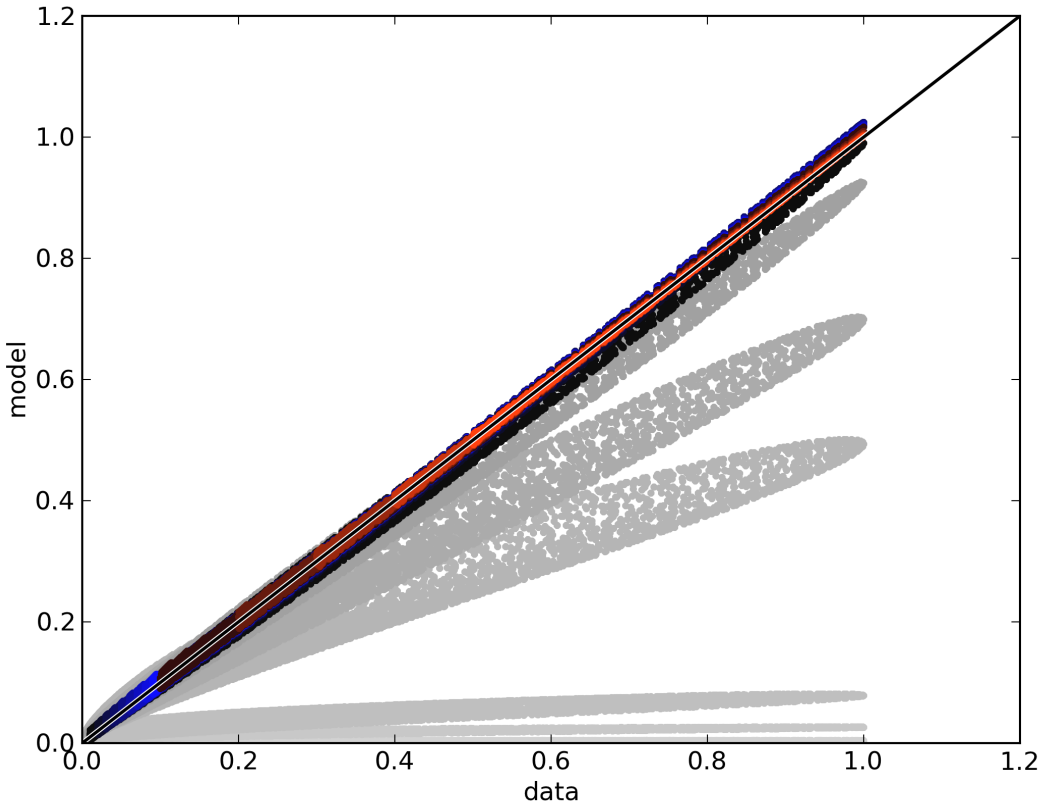

Figure 10: Model from a gaussian fit v.z. GRASP map for 70 GHz, FH18X. Both model and data are normalized to be 1 at the peak value. Red dots: data for threshold from 0.1 to 0.5. Blue dots: data for threshold from 0.01 to 0.0.9. Gray dots: data for threshold 10^{-6}, 5×10^{-6}, 10^{-5}, 5×10^{-5}, 10^{-4}, 5×10^{-4}, 10^{-3}, 5×10^{-3}.

the model assumes that no baseline is present in the "data", i.e. the GRASP maps, this is reasonable since the GRASP beam maps does not contain any sky or anything else from the beam itself. The assumption allows to fit data with Eq. (20) with an analytical solution which does not require any prior.

Free parameters of the model are

1. U_0, V_0 the center of the gaussian fit in arcsec
2. $\mathrm{fwhm} = \sqrt{\mathrm{fwhm_{max}}\mathrm{fwhm_{min}}}$ in deg
3. the ellipticity $\epsilon_\mathrm{g} = \mathrm{fwhm_{max}}/\mathrm{fwhm_{min}}$
4. ψ_ell in deg, the tilt of the major axis about the U axis.
5. g_0 the peak value.

Given the GRASP beams does not follow exactly a gaussian, there is the need to put a threshold on the minimum value acceptable within the map. Parameters as g_0 drop suddenly when data in the (U, V) plane for which $G_\mathrm{m}(U, V) < 0.05 G_\mathrm{m}(0, 0)$ are taken, since the whole beam is rather platocurtic with respect to a true gaussian beam. Fig. 10 shows predicted $G_\mathrm{m}(U, V)$ from the gaussian fit Eq. (20) v.z. the beam values in the original GRASP map. Colours represents the level of threshold by which pixels in the original GRASP map have been selected. So a threshold 0.5 or 0.1 means that the fit have been perfomed by taking pixels whose value is lager than 0.5 or 0.1 time the map peak value. In the ideal case the points should fall on the black line. Indeed it is evident how down to a threshold of 0.01 the gaussian fit performs well, after that the model departs significantly from the GRASP with larger and larger departures the threshold decreases. **However since we are interested in looking at the propagation of uncertainties rather than at predicting an exact value, we perform the fit just taking data for which** $G_\mathrm{m}(U, V)/G_\mathrm{m}(0, 0) \geq 0.1$ [5] Within this range the values of gaussian fit parameters, and more important, their relative variability, are largely insensitive to the exact value of the threshold.

5.3 Results

Montecarlo shows that the distribution of randomly generated parameters is gaussian with expectation given by the corresponding value for nominal RIMO, the corresponding RMS scales as $\delta_\mathrm{db} \log \tau$ and it is approximately invariant with α.

Figures 11, 12, 13, 14, 15 compares the variation of Gaussian fitting parameters in the original GRASP maps as a function of frequency with the corresponding quantities as a function of α after having averaged the frequency maps over the bandwidth. The plot share the same vertical scale, but the horizontal scale depends on the symbols. Triangles are values derived from the original GRASP maps computed at specific frequencies given by the bottom scale. Circles (with error bars) are values derived from the frequency averaged maps as a function of α given by the top scale. Note that the two horizontal scales are not correlated, i.e. there is not relation between α and ν. The horizontal lines are the values for the parameter for the reference frequency, in this case 30 GHz. The errorbars are calculated for $\delta_\mathrm{db} \log \tau = 2\sqrt{12}$db.

Tables 1, 2 and 3 gives for each parameter P:

$P(\alpha)$ the value for average over a flat spectrum $\alpha = 0$;

[5] This is equivalent at stopping the fitting at 10db from the peak, this is not the procedure used to derive values in the focal plane database, but since the scope is to derive the relative variability, we considered this approximation sufficient for the scopes of the current Issue of this document.

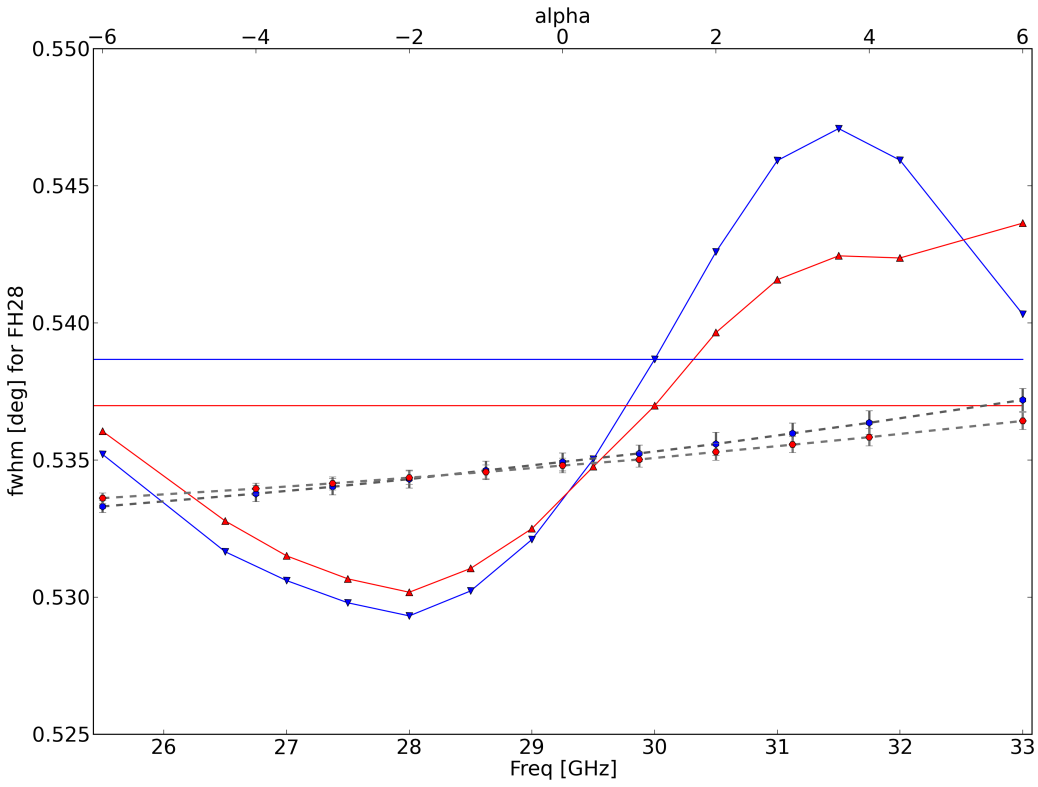

Figure 11: fwhm from GRASP maps as a function of frequency (triangles - refers to the bottom horizontal scale), and from frequency averaged maps as a function of α (circles - referes to the top horizontal scale). The two horizontal scales are not related. i.e. α is not a function of frequency. Blue is for X polarization, red is for Y polarization. Errorbars are calculated for $\delta_{\rm db} \log \tau = 2\sqrt{12}$db. The figure refer to FH 28, the reference frequency is 30 GHz, the horizontal lines denotes the values for the two polarizations at the reference frequency.

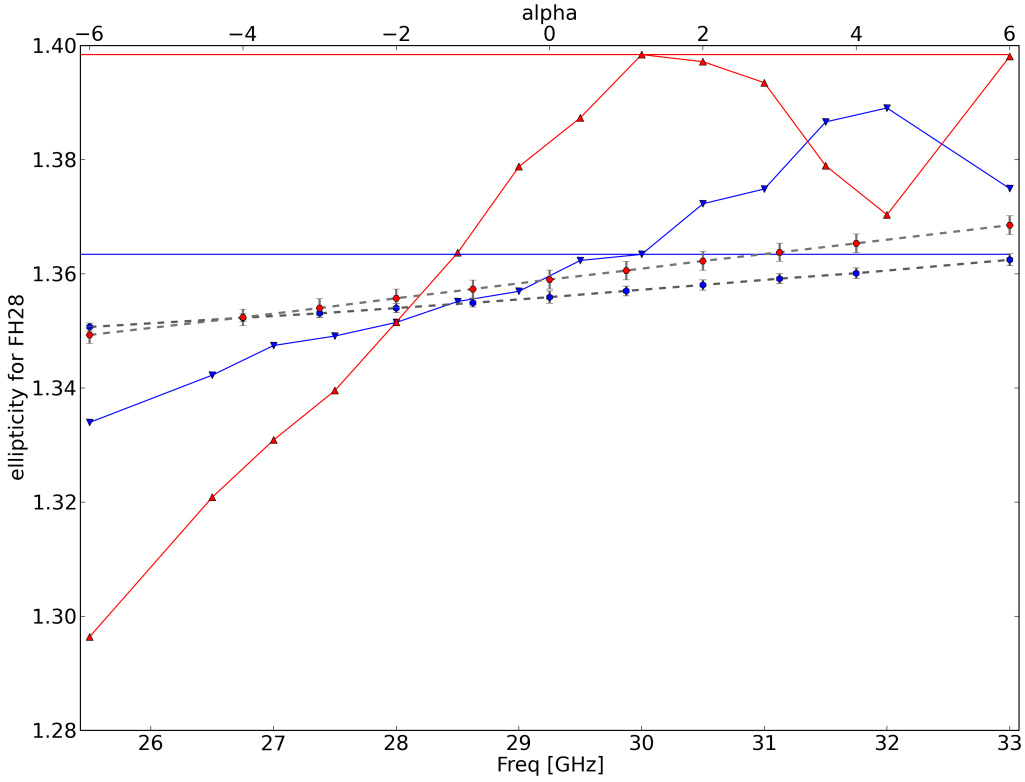

Figure 12: Ellipticity from GRASP maps and frequecy integrated maps. See Fig. 11 for details.

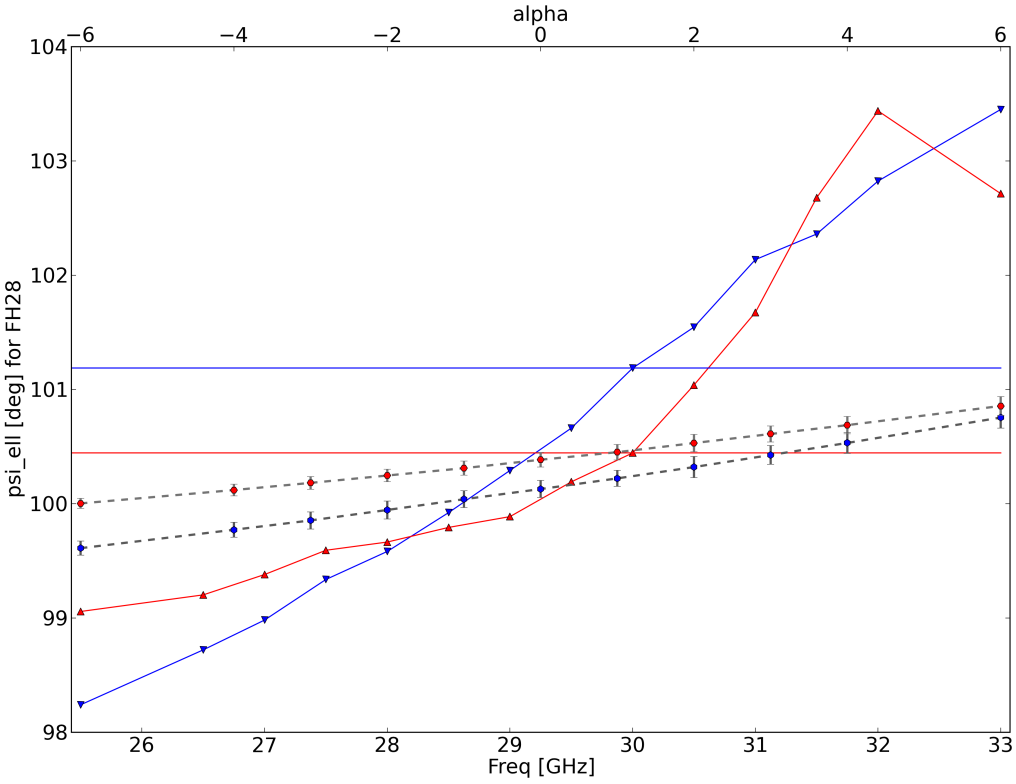

Figure 13: $\psi_{\rm ell}$ from GRASP maps and frequecy integrated maps. See Fig. 11 for details.

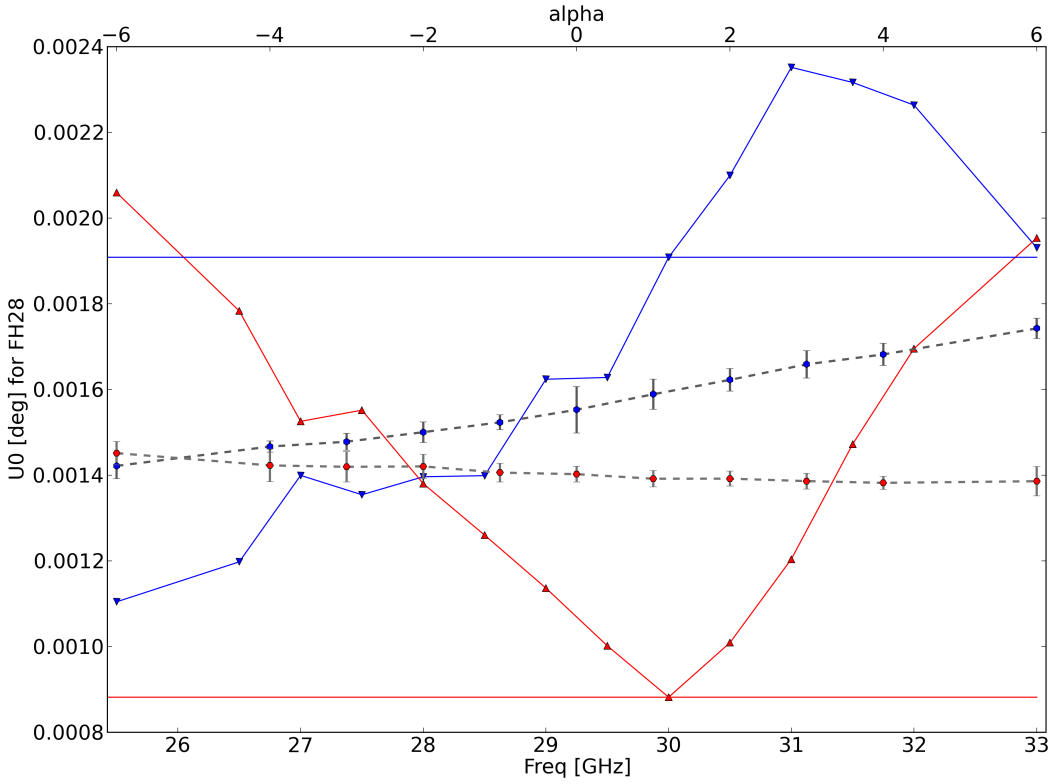

Figure 14: U_0 from GRASP maps and frequecy integrated maps. See Fig. 11 for details.

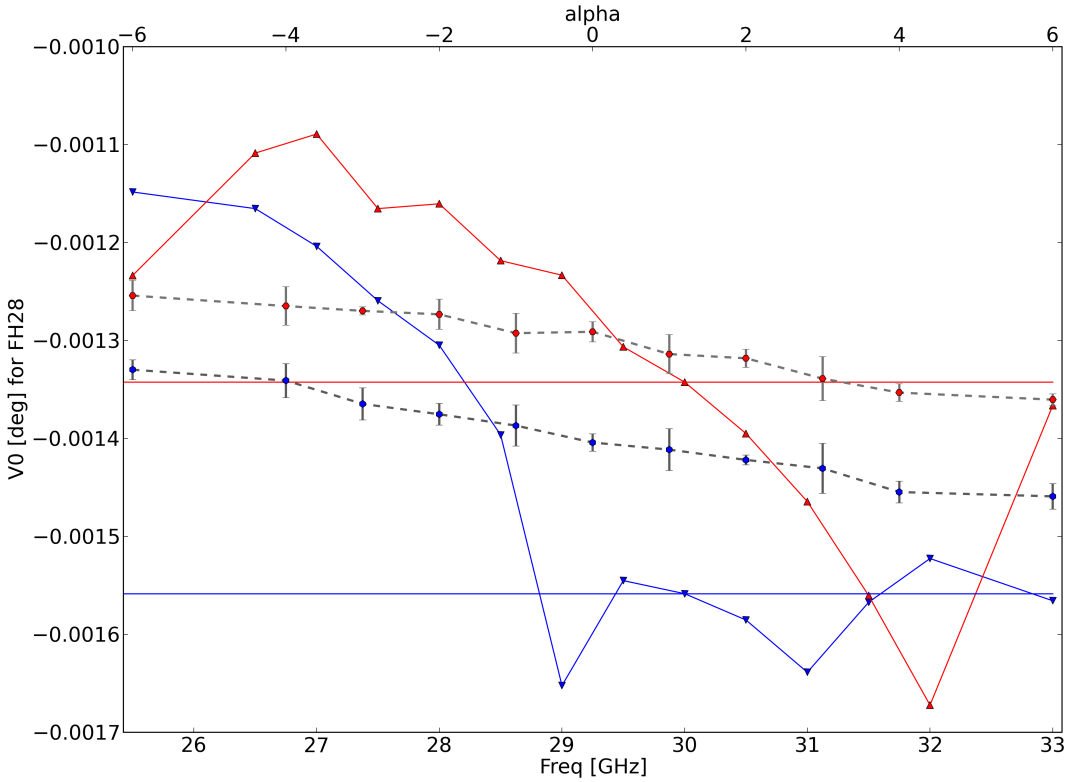

Figure 15: V_0 from GRASP maps and frequecy integrated maps. See Fig. 11 for details.

$\sigma_P(\alpha)$ the value for the RMS from $n_{\rm mc} = 2500$ montecarlos for $\delta_{\rm db} \log \tau = 2$ db;

$\partial P/\partial\alpha$ the slope of P variation as a function of α.

Given the uncertainties are derived for $\delta_{\rm db} \log \tau = 2$ db it is convenient to give the relative uncertainty in units of %/db In summary it is possible to state that.

1. All the free parameters changes with frequency (for the GRASP maps) and with α, but Bandpass averaging reduces the level of variability of each parameter at least in the considered $-6 \leq \alpha \leq +6$ intervall.

2. the U_0 and V_0 changes of up to 0.2 arcsec for each unit of α, the level of uncertainty is less than 8×10^{-3} $arcsec$/db.

3. the fwhm changes of about $(3 \times 10^{-4})^\circ/\alpha$. The sign depend on the slope, the peak–to–peak variation in the fwhm is about $(3.6 \times 10^{-3})^\circ$ or about less than 2% of the fwhm at $\alpha = 0$. The uncertainty is less than $(4 \times 10^{-5})^\circ$/db or 0.02%/db;

4. similar orders of magnitude appears for the ellipticity;

5. At last $\psi_{\rm ell}$ changes of up to 4.3° with α, with an uncertainty of up to $(3 \times 10^{-2})^\circ$/db.

It is not easy to combine all of this information to understand the impact on photometric accuracy. Possible combined parameters are the product $\Delta\nu_{\rm eff} f_{\rm c}^2$ and the ratio $G_{T{\rm ant}2W}$ of Eq. (**??**) computed at peak value of the beam, both of which are tabulated in Tab. 5. Even here the uncertainty impacts at the level of 0.2%/db, while α introduces a variation of up to the 10% peak-to-peak.

	U_0 [arcsec]			V_0 [arcsec]		
FH	$U_0(\alpha=0)$	σ_{U_0}	$\partial U_0/\partial\alpha$	$V_0(\alpha=0)$	σ_{V_0}	$\partial V_0/\partial\alpha$
18x	0.95	6.95e-03	7.76e-03	3.22	7.14e-03	5.59e-02
18y	1.38	1.71e-02	-1.51e-03	2.91	6.81e-03	2.44e-02
19x	2.24	6.96e-03	3.12e-02	1.95	4.83e-03	2.26e-02
19y	2.85	7.39e-03	-1.79e-02	1.36	5.99e-03	1.02e-02
20x	1.53	4.55e-03	3.68e-02	0.17	4.61e-03	-7.59e-03
20y	1.65	3.97e-03	-2.34e-02	-0.21	1.28e-02	-5.00e-04
21x	1.51	6.86e-03	1.97e-02	-0.35	4.39e-03	8.54e-03
21y	1.68	6.18e-03	-2.03e-02	0.14	5.04e-03	-1.67e-02
22x	3.13	9.03e-03	3.68e-02	-1.99	3.81e-03	-3.09e-02
22y	3.37	4.79e-03	7.37e-03	-1.56	5.90e-03	-2.23e-02
23x	1.07	4.40e-03	1.77e-02	-3.56	9.77e-03	-5.04e-02
23y	1.30	1.14e-02	1.05e-02	-3.13	5.69e-03	-3.39e-02
24x	5.77	1.37e-02	6.23e-02	-0.06	8.45e-03	-2.49e-03
24y	4.51	5.14e-03	1.87e-02	-0.05	2.26e-03	5.58e-03
25x	-16.24	2.85e-02	-1.24e-01	30.07	1.67e-02	-6.56e-02
25y	-16.24	4.11e-02	-1.62e-01	28.82	1.92e-02	-8.44e-02
26x	-14.39	2.33e-02	-9.78e-02	-30.25	1.93e-02	5.88e-02
26y	-14.54	2.82e-02	-1.67e-01	-28.94	1.49e-02	1.01e-01
27x	5.85	1.65e-02	9.83e-02	5.18	1.91e-02	4.99e-02
27y	5.43	2.25e-02	-3.05e-02	4.73	7.28e-03	2.49e-02
28x	5.59	3.15e-02	9.08e-02	-5.05	5.24e-03	-4.40e-02
28y	5.05	1.16e-02	-2.12e-02	-4.65	6.32e-03	-3.54e-02

Table 1: Prediction uncertainty for U_0 and V_0 as a function of α for $\delta_{\rm db}\log\tau = 2$db.

	FWHM [deg]			ϵ_g		
FH	FWHM($\alpha=0$)	$\sigma_{\rm FWHM}$	∂FWHM/$\partial\alpha$	$\epsilon_g(\alpha=0)$	σ_{ϵ_g}	$\partial\epsilon_g/\partial\alpha$
18x	0.220289	1.86e-05	-1.27e-04	1.270217	6.28e-05	3.83e-05
18y	0.219344	1.58e-05	-1.08e-04	1.228574	6.71e-05	3.54e-04
19x	0.213921	1.53e-05	-8.93e-05	1.273542	5.20e-05	-2.81e-04
19y	0.214422	2.28e-05	-1.41e-04	1.238834	5.49e-05	2.78e-04
20x	0.210580	2.26e-05	-1.53e-04	1.276224	1.58e-04	-5.59e-04
20y	0.210135	2.49e-05	-1.58e-04	1.262139	7.18e-05	1.21e-04
21x	0.211400	2.65e-05	-1.53e-04	1.277795	9.28e-05	-6.81e-04
21y	0.210216	2.82e-05	-2.31e-04	1.261246	3.79e-05	2.25e-04
22x	0.214349	1.45e-05	-1.12e-04	1.272690	8.58e-05	-5.33e-04
22y	0.213433	1.80e-05	-1.49e-04	1.244337	7.04e-05	4.05e-04
23x	0.220278	1.14e-05	-9.26e-05	1.273966	3.26e-05	1.21e-04
23y	0.219336	1.65e-05	-1.07e-04	1.231544	6.50e-05	3.10e-04
24x	0.376165	4.13e-05	1.40e-04	1.300924	2.58e-04	-6.84e-04
24y	0.380629	5.36e-05	2.15e-04	1.401267	6.03e-04	2.40e-03
25x	0.504620	2.94e-05	6.53e-05	1.221841	1.01e-04	-7.28e-04
25y	0.492340	5.25e-05	-2.80e-04	1.232849	2.87e-04	-1.28e-03
26x	0.505714	3.24e-05	5.68e-05	1.223249	1.23e-04	-7.16e-04
26y	0.493350	5.62e-05	-3.35e-04	1.234492	2.50e-04	-1.40e-03
27x	0.535062	7.19e-05	2.96e-04	1.357922	1.49e-04	8.86e-04
27y	0.534248	4.99e-05	1.75e-04	1.354692	2.96e-04	1.52e-03
28x	0.534932	8.42e-05	3.00e-04	1.355923	1.99e-04	9.54e-04
28y	0.534801	6.67e-05	2.20e-04	1.359006	3.26e-04	1.65e-03

Table 2: Prediction uncertainty for U_0 and V_0 as a function of α for $\delta_{\rm db}\log\tau = 2$db.

	$\psi_{\rm ell}$ [deg]		
FH	$\psi_{\rm ell}(\alpha=0)$	$\sigma_{\psi_{\rm ell}}$	$\partial\psi_{\rm ell}/\partial\alpha$
18x	-89.538697	3.03e-02	1.60e-01
18y	89.761491	6.41e-02	1.29e-01
19x	-81.433995	1.15e-02	6.32e-02
19y	-80.965641	1.04e-02	6.80e-02
20x	-73.481212	8.63e-03	5.43e-02
20y	-72.759836	1.07e-02	-9.68e-03
21x	73.757710	9.89e-03	-5.77e-02
21y	72.813754	5.85e-03	3.15e-03
22x	81.063648	1.45e-02	-9.63e-02
22y	80.259396	1.08e-02	-7.57e-02
23x	89.650159	2.01e-02	-1.20e-01
23y	89.418085	2.88e-02	-1.22e-01
24x	-89.976640	1.86e-03	-1.93e-04
24y	-89.988365	2.43e-04	-8.22e-04
25x	65.321276	6.72e-02	-3.32e-01
25y	66.851747	7.94e-02	-3.32e-01
26x	-66.055394	6.10e-02	2.88e-01
26y	-67.259548	7.18e-02	3.61e-01
27x	79.780143	1.58e-02	-8.60e-02
27y	79.849117	1.42e-02	-6.09e-02
28x	-79.871173	1.82e-02	9.09e-02
28y	-79.614589	1.59e-02	6.81e-02

Table 3: Prediction uncertainty for $\psi_{\rm ell}$ as a function of α for $\delta_{\rm db}\log\tau = 2$db.

	Fc [GHz]			$\Delta\nu_{\rm eff}$ [GHz]		
FH	$Fc(\alpha=0)$	σ_{Fc}	$\partial Fc/\partial\alpha$	$\Delta\nu_{\rm eff}(\alpha=0)$	$\sigma_{\Delta\nu_{\rm eff}}$	$\partial\Delta\nu_{\rm eff}/\partial\alpha$
18x	70.24	3.86e-02	3.04e-01	15.98	4.54e-02	-1.37e-02
18y	69.82	2.48e-02	1.96e-01	12.76	4.63e-02	-2.90e-02
19x	70.40	2.10e-02	1.75e-01	11.99	5.02e-02	-9.75e-02
19y	68.85	2.62e-02	1.91e-01	12.61	4.73e-02	4.12e-02
20x	70.29	2.38e-02	2.02e-01	12.89	5.32e-02	-9.80e-02
20y	70.12	2.27e-02	1.88e-01	12.45	5.25e-02	-7.18e-02
21x	69.57	2.59e-02	2.05e-01	13.09	4.69e-02	1.85e-02
21y	70.36	3.44e-02	2.76e-01	15.21	4.36e-02	-3.44e-02
22x	71.27	2.85e-02	2.45e-01	14.20	5.31e-02	-1.88e-01
22y	71.09	2.54e-02	2.24e-01	13.54	5.57e-02	-1.94e-01
23x	71.29	2.50e-02	2.18e-01	13.33	5.43e-02	-2.16e-01
23y	70.82	2.23e-02	1.94e-01	12.55	5.59e-02	-1.82e-01
24x	43.80	2.23e-02	1.28e-01	8.21	4.40e-02	6.88e-03
24y	44.24	2.16e-02	1.21e-01	7.97	3.48e-02	-2.91e-02
25x	44.01	2.00e-02	1.16e-01	7.77	3.98e-02	-4.25e-02
25y	43.99	2.00e-02	1.14e-01	7.74	3.78e-02	-1.74e-02
26x	43.91	1.88e-02	1.03e-01	7.33	3.57e-02	-2.32e-02
26y	43.99	2.53e-02	1.45e-01	8.65	5.89e-02	-7.00e-02
27x	28.63	2.20e-02	1.21e-01	6.61	2.80e-02	1.13e-01
27y	28.40	2.03e-02	1.04e-01	6.14	2.88e-02	1.21e-01
28x	28.41	2.29e-02	1.30e-01	6.87	2.92e-02	1.33e-01
28y	28.74	2.18e-02	1.20e-01	6.57	2.67e-02	9.42e-02

Table 4: Prediction uncertainty for Fc and $\Delta\nu_{\rm eff}$ as a function of α for $\delta_{\rm db}\log\tau = 2$db.

	$\Delta\nu_{\rm eff} f_{\rm c}^2$ [GHz]			$G_{T\rm ant2W}$ [GHz]		
FH	$\Delta\nu_{\rm eff} f_{\rm c}^2(\alpha=0)$	$\sigma_{\Delta\nu_{\rm eff} f_{\rm c}^2}$	$\partial\Delta\nu_{\rm eff} f_{\rm c}^2/\partial\alpha$	$G_{T\rm ant2W}(\alpha=0)$	$\sigma_{TantTpow}$	$\partial G_{T\rm ant2W}/\partial\alpha$
18x	78836.47	2.04e+02	5.79e+02	540363851.23	1.39e+06	4.55e+06
18y	62189.27	2.15e+02	2.06e+02	429942164.29	1.46e+06	1.84e+06
19x	59415.76	2.47e+02	-1.83e+02	431856979.20	1.77e+06	-9.62e+05
19y	59765.75	2.10e+02	5.20e+02	432375225.00	1.49e+06	4.31e+06
20x	63666.27	2.55e+02	-1.12e+02	477552249.75	1.87e+06	-1.49e+05
20y	61208.60	2.53e+02	-2.10e+01	461063379.05	1.87e+06	5.36e+05
21x	63331.54	2.24e+02	4.57e+02	471360998.09	1.64e+06	4.06e+06
21y	75318.69	2.00e+02	4.01e+02	566915591.21	1.50e+06	4.20e+06
22x	72125.78	2.51e+02	-4.49e+02	522148908.36	1.78e+06	-2.70e+06
22y	68402.17	2.68e+02	-5.34e+02	499450214.38	1.92e+06	-3.18e+06
23x	67735.45	2.60e+02	-6.67e+02	464321886.87	1.76e+06	-4.17e+06
23y	62942.35	2.70e+02	-5.56e+02	435180190.08	1.84e+06	-3.41e+06
24x	15741.61	8.62e+01	1.05e+02	37003094.99	2.00e+05	2.19e+05
24y	15593.11	6.95e+01	2.87e+01	35799211.29	1.57e+05	2.56e+04
25x	15046.29	7.54e+01	-1.96e+00	19653808.80	9.81e+04	-7.56e+03
25y	14966.76	7.44e+01	4.44e+01	20537321.80	1.03e+05	8.40e+04
26x	14124.04	6.86e+01	2.18e+01	18369413.30	8.89e+04	2.43e+04
26y	16743.15	1.06e+02	-2.19e+01	22880835.04	1.43e+05	1.10e+03
27x	5422.74	2.83e+01	1.37e+02	6300204.72	3.15e+04	1.53e+05
27y	4948.29	2.83e+01	1.33e+02	5766513.92	3.20e+04	1.51e+05
28x	5542.32	2.90e+01	1.57e+02	6442269.50	3.20e+04	1.75e+05
28y	5428.81	2.66e+01	1.22e+02	6313424.83	2.99e+04	1.37e+05

Table 5: Prediction uncertainty for Fc and $\Delta\nu_{\rm eff}$ as a function of α for $\delta_{\rm db}\log\tau = 2$db.

A Reflection Loss

The maps produced by the GRASP code does not introduce the reflection losses of the mirrors. Reflection losses are dominated by resistive dissipation on the telescope surface. So the fraction of absorbed energy is proportional to the $\rho_\Omega(T,\nu)$ of the surface. There are not direct measures at LFI frequencies but in [RD-1] it is shown that above 100 GHz the skin–effect is the dominating effect defining $\rho_\Omega(T,\nu)$ so the resistivity will scale as $\sqrt{(}\nu)$ or

$$\mathcal{R}_{\rm loss} = 1 - \dot{\mathcal{R}}_{\rm loss}(T)\left(\frac{\nu}{141.4\ {\rm GHz}}\right)^{0.5} \tag{21}$$

with a slope $\dot{\mathcal{R}}_{\rm loss}(T)$ depending on the temperature. [RD-1] reports in their Fig.B.1 at 141.4 GHz, 120°K temperature, $1-\mathcal{R}_{\rm loss} \approx 0.93\times10^{-3}$. It is not easy to scale down this at the telescope operative temperatures ($\approx 45K$) becouse the anomalous skin–effect flattens the temperature dependence of $\dot{\mathcal{R}}_{\rm loss}(T)$. However, Fig.B.1 suggests $\dot{\mathcal{R}}_{\rm loss}(50K)$ between 0.7 - 0.9. Also at begin of the same appendix it is quoted an estimated reflection–loss at 50 GHz and 120 K of $\approx 0.05\%$ consistent with the aforementioned slope. With these figures, assuming conservatively $\dot{\mathcal{R}}_{\rm loss}(50K) \approx \dot{\mathcal{R}}_{\rm loss}(120K)$, and neglecting second order terms of order $\dot{\mathcal{R}}^2_{\rm loss} \approx 10^{-6}$, the global reflection loss for primary and secondary mirror will be

$$\mathcal{R}_{\rm loss,tel} = 1 - 1.4\times10^{-4}\left[\frac{\nu}{1\ {\rm GHz}}\right]^{0.5} \tag{22}$$

so, as an example, at 30 GHz assuming a 20% bandwidth the reflectivity will change of a fraction $\pm 1.5\times10^{-4}$ across the band.